Spatially programmable wave compression and signal enhancement in a piezoelectric metamaterial waveguide

Christopher Sugino[*]

Department of Mechanical Engineering, Charles V. Schaefer, Jr. School of Engineering and Science,
Stevens Institute of Technology, Hoboken, New Jersey 07030, USA

Mustafa Alshaqaq and Alper Erturk

G.W. Woodruff School of Mechanical Engineering, Georgia Institute of Technology, Atlanta, Georgia 30332, USA

We demonstrate high-precision dispersion tailoring in a metamaterial waveguide for wave compression and spatially tunable signal amplification. Spatial control over refractive index is achieved via digital controllers connected to piezoelectric unit cells. The digital shunt circuits allow numerically optimized circuit parameters to be uploaded directly to the experimental platform, enabling arbitrary spatial programming of the refractive index of the waveguide. Thus, the system acts as a reconfigurable piezoelectric array, altering the wavelength and group velocity of a given wave according to user specifications. In this work, optimizations are performed to implement gradual wave compression, realizing an effect analogous to that of an acoustic black hole. At the operating frequency of the design, the waveguide exhibits increased sensitivity and amplification of piezoelectric voltage output due to the compressed wavelength, shunt circuit resonance, and gradual variation in unit cell properties, avoiding internal reflections. Numerical and experimental results show that voltage amplification can be achieved in a desired position and frequency in the metamaterial waveguide.

I. INTRODUCTION

Elastic and acoustic metamaterials, architected structures made from a repeated unit cell, promise to expand the realm of possibilities in wave physics with applications from vibration and noise control to wave devices. Metamaterials exhibit exotic effective properties not found in nature, such as negative dynamic mass [1–3] or negative dynamic stiffness and modulus [4–6], that dramatically affect their dynamic behavior. Many studies on these systems are limited to uniform metamaterials with identical unit cells [1–8]. Varying unit cells in space yields gradient metamaterials [9–12], wherein dispersion properties are gradually varied in space to steer, focus, or compress propagating waves. Such smooth spatial variation is required, for example, to achieve acoustic and elastic cloaking [13–16] without excessive reflections.

A promising application of gradient metamaterials is the enhancement of acoustic sensing via wave compression [17]. Compression of waves in space corresponds to an increase in the local concentration of energy, increasing potential sensor output at that location. This is conceptually similar to an acoustic black hole [18–24], in which waves are slowed down (theoretically to zero velocity), corresponding to a decreased wavelength and increased amplitude. However, such devices have typically relied on a fixed geometry (e.g., a machined feature with smooth geometric variation) or gradient architecture. Piezoelectric metamaterials, by contrast, have effective properties that depend on an electrical circuit [6,25–28],

providing a mechanism to achieve multiple gradient configurations in a single experimental platform [29,30], especially when combined with digitally programmable shunt circuitry, or synthetic impedance [31–35].

In this paper, we present numerical and experimental analysis of a waveguide with programmable wave compression. We build upon our previous work with a similar experimental platform [35] (here, a separate beam with different boundary conditions and less damping), establishing a procedure to (1) calculate the impedance required for a desired refractive index profile, and (2) apply it directly to the experimental platform. As such, the developed system is a major step toward *programmable* wave devices, providing a direct path from desired wave behavior to the physical system. This significantly advances the multifunctionality of metamaterial wave-compression devices, providing signal enhancement at a programmable frequency and position in the waveguide.

II. PIEZOELECTRIC METAMATERIAL DESIGN AND NUMERICAL RESULTS

We consider a piezoelectric metamaterial waveguide comprising an aluminum beam with separately bonded piezoelectric patches (piezos) [Fig. 1(a)]. Each pair of symmetrically bonded identical piezos has the same poling direction for standard parallel-wire operation under flexural vibration. The external electrodes of each pair of piezos are electrically connected, and the central shim forms the negative electrode for all of piezos in the metamaterial. Each pair of piezos is shunted to a separate circuit with admittance Y_j, here provided a synthetic impedance circuit [31,33]. By varying the
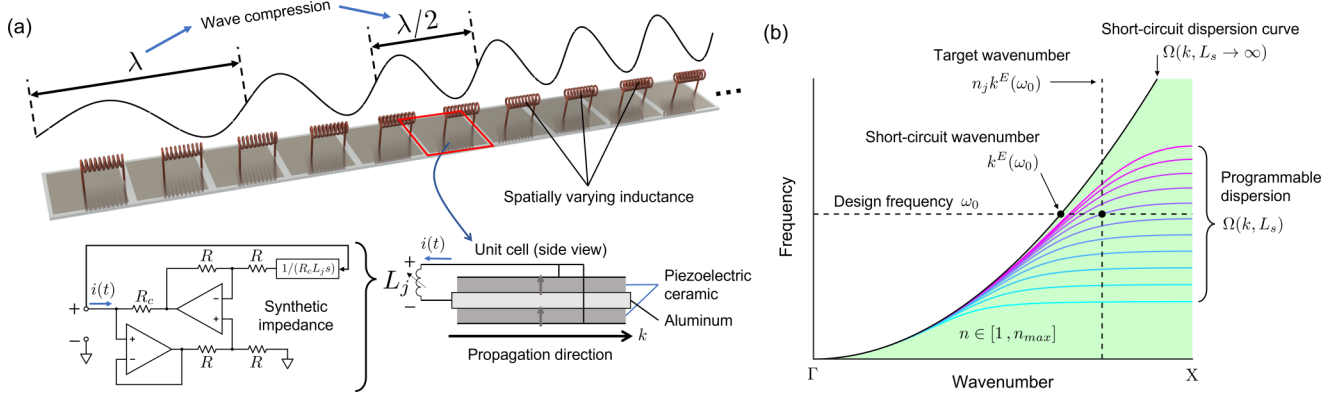
---
[*]csugino@stevens.edu

FIG. 1. (a) Schematic of the programmable piezoelectric metamaterial. Synthetic impedance circuits are used as shunt circuits to enable free spatial variation of the shunt inductance. (b) Variation of the shunt inductance enables the dispersion of the waveguide to be varied throughout the green shaded region.

admittance Y_j of each unit cell, the local dispersion relation in the waveguide can be smoothly varied [Fig. 1(b)].

A finite element model of the unit cell of the metamaterial was constructed in COMSOL Multiphysics, shown schematically in Fig. 1(a). The unit cell consists of a single pair of piezoelectric patches and the aluminum shim, reduced in half by symmetry, with Floquet boundary conditions in the x direction and all other boundaries kept free. An inductor with inductance L_s is connected between the piezoelectric electrodes and the central shim, such that $Y(i\omega) = 1/(i\omega L_s)$. For one-dimensional wave propagation with wave number k, the irreducible Brillouin zone (IBZ) is $k \in [0, \pi/a]$, where a is the unit cell size in the propagation direction. The dispersion curves can be computed directly as $\Omega(k, L_s)$, where Ω are the eigenvalues of the system at wave number k and shunt inductance L_s. The inductance L_s changes the dispersion curves of the system dramatically near the inductive-capacitive (LC) resonant frequency of the unit cell.

To achieve wave compression, we follow an approach analogous to an acoustic black hole [18–24], wherein waves are gradually slowed down by smoothly varying a system parameter (e.g., thickness or a unit cell property). Because the metamaterial comprises discrete unit cells, it is convenient to use refractive index to identify the parameters required in each unit cell to achieve gradual reduction in wavelength [20]. At a given frequency ω, the refractive index is defined as $n = k(\omega)/k^E(\omega) = \lambda^E(\omega)/\lambda(\omega)$, where $k^E(\omega)$ is the short-circuit wave number, $\lambda^E(\omega) = 2\pi/k^E(\omega)$ is the short-circuit wavelength, and $\lambda(\omega) = 2\pi/k(\omega)$ is the wavelength in the shunted unit cell. To achieve linear reduction in wavelength, we consider a refractive index profile [20]

$$n_j = \frac{n_1 n_N}{n_N - (n_N - n_1)(j-1)/(N-1)}, \quad j = 1 \ldots N, \quad (1)$$

where N is the total number of unit cells, (n_1, n_N) are the designed minimum and maximum refractive indices, and the dependence of refractive index on frequency and unit-cell inductance has been omitted for clarity. Note that, while the following analysis focuses on this specific refractive index profile, the same approach could be used to implement other refractive index profiles, such as to achieve maximum compression mid-span along the waveguide. Due to the discrete

nature of the metamaterial's unit cells, the refractive index cannot vary completely smoothly; however, provided that there are a large number of unit cells, the properties of adjacent unit cells can be kept relatively similar to avoid undesired wave reflections. This assumption will later be validated using simulations of the full, finite system with nonuniform unit cells.

The maximum wave number that can be achieved by unit-cell based techniques is $k_{\max} = \pi/a$, where a is the unit cell size, corresponding to the right edge of the IBZ. Additionally, because we only consider the lowest dispersion branch and inductive shunt circuits, the wave number can only be *increased* beyond its short-circuit value [see Fig. 1(b)]. Thus, the wave number of the shunted unit cell can only be in the range $k \in [k^E, \pi/a]$, and hence the range of achievable refractive indices for each shunted unit cell is $n_j \in [1, \pi/(ak^E)]$. Other shunt circuit types such as negative capacitance could be used to increase the wave speed and increase the wavelength, but this is beyond the scope of this work.

To calculate the required inductance L_j to obtain the refractive index profile n_j at the selected operating frequency ω_0, first the short-circuit wave number $k^E(\omega_0)$ is computed through numerical optimization, i.e.,

$$k^E(\omega_0) = \arg\min_k [\omega_0 - \Omega(k, L_s \to \infty)]^2, \quad (2)$$

where $L_s \to \infty$ indicates that the electrodes are short-circuited to the central shim. Next, N optimizations are performed to obtain the inductance values L_j that yield the desired refractive indices:

$$L_j = \arg\min_{L_s} [\omega_0 - \Omega(n_j k^E(\omega_0), L_s)]^2, \quad (3)$$

where $n_j k^E(\omega_0)$ is the wave number corresponding to the desired refractive index. Note that the calculated inductance values are those of the symmetry-reduced unit cell; the actual shunt inductance is half of the calculated value. The numerical calculation procedure for the inductance profile is shown in Fig. 1(b), along with typical unit cell dispersion curves. This procedure was used to calculate the required inductance profile for $n_1 = 1.02$, $n_N = 3.5$ at an operating frequency of 1250 Hz.

The inductance profile L_j corresponds to a family of dispersion curves $\Omega(k, L_j)$ that represent the variation of
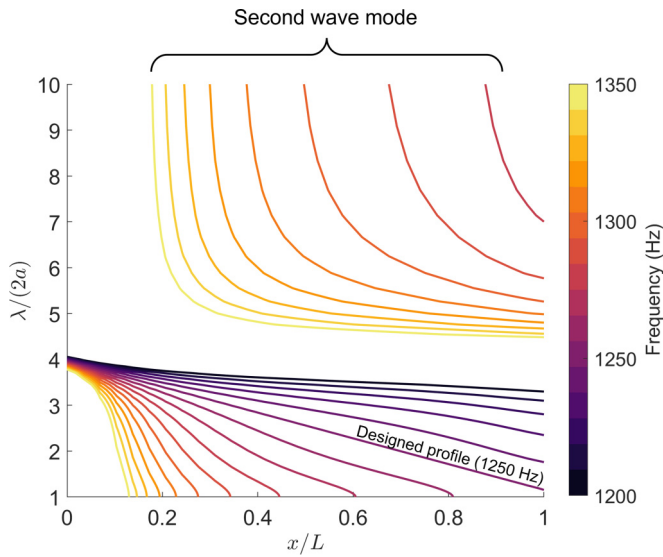
FIG. 2. Wavelength vs position at various frequencies using the inductance profile calculated for 1250 Hz propagation.
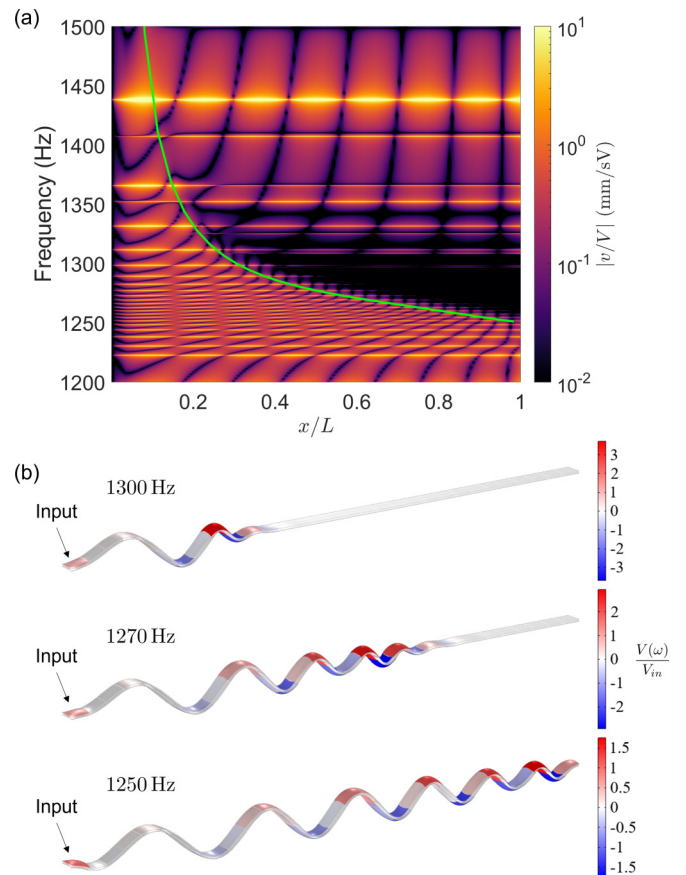

FIG. 3. (a) Simulated steady-state response of the metamaterial vs position and frequency. The green line indicates the resonant frequencies of the unit cells. (b) Beam response at selected frequencies highlighting the wave compression and varying cutoff position.

local dispersion properties along the modulated section of the waveguide. These dispersion curves can be used to describe the behavior of the waveguide at frequencies other than the chosen operating frequency. For example, it is useful to consider the wavelength variation along the waveguide at various frequencies, as shown in Fig. 2. The wavelength contours show that the calculated inductance profile gives smooth reduction in wavelength at the operating frequency (1250 Hz), resulting in a roughly four-times reduction wavelength from one end of the waveguide to the other. At frequencies above the operating frequency, the wavelength is reduced up to a certain position in the waveguide before increasing rapidly as the first dispersion branch terminates and the second dispersion branch is excited. At frequencies below the operating frequency, the wavelength still decreases along the waveguide, but the variation in wavelength is reduced.

The dispersion-based predictions of the preceding analysis may become inaccurate for a gradient metamaterial with rapidly changing effective properties. Additionally, the experimental system is a finite size and has a limited number of unit cells available, such that the boundary conditions of the structure may become important. Thus, a finite-element model of the finite-size metamaterial system was constructed to match the experimental setup using the numerically calculated inductance profile. The steady-state velocity of the waveguide is shown versus frequency and space in Fig. 3(a). The waveguide velocity is shown at selected frequencies in Fig. 3(b), along with the voltage on each piezoelectric patch. As predicted from the wavelength contours of Fig. 2, wave compression occurs up to a certain position that depends on frequency. Additionally, the voltage output of the piezoelectric patches increases up until the point of maximum compression, corresponding to the resonant behavior of each unit cell, while the amplitude of motion gradually decreases. Unlike a conventional machined acoustic black hole, in which wave compression yields an increase in velocity amplitude, the piezoelectric metamaterial concentrates wave

energy primarily in the electrical domain. However, similar to an acoustic black hole, the smooth variation in unit cell properties forms a type of matching layer, increasing the signal output (i.e., piezoelectric voltage) by gradually slowing down the incident wave and avoiding intermediate reflections. Finally, the close correspondence between the predictions of Fig. 2, which were derived using unit-cell based analysis, and the steady-state response in Fig. 3(b) suggests that the metamaterial gradient is sufficiently gradual to avoid significant internal reflections.

III. EXPERIMENTAL RESULTS

A piezoelectric waveguide with 31 unit cells was fabricated using an aluminum shim (0.32 m × 1 cm × 0.8 mm) and 31 pairs of piezoelectric patches (1 cm × 1 cm × 0.31 mm) from APC (material APC 850, similar to PZT-5A) with 0.25 mm between each piezoelectric patch. The piezoelectric patches were bonded with the same poling orientation for parallel wire operation, i.e., the opposing electrodes of each unit cell were electrically connected and shunted [see Fig. 1(a)], while the internal electrodes were grounded to the central shim. Each piezoelectric patch was vacuum-bonded to the aluminum shim to minimize the bonding layer thickness, achieving significantly reduced damping compared
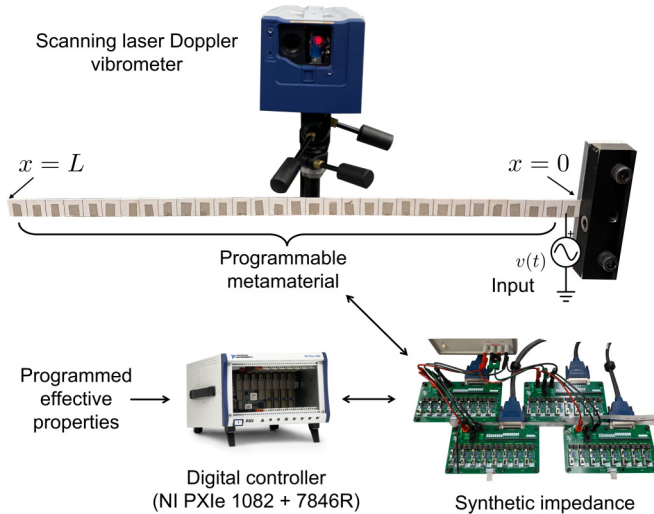
FIG. 4. Experimental realization of the programmable piezoelectric metamaterial. Synthetic impedance is used to enable spatial programming of the inductance applied to each unit cell.

to our previous programmable piezoelectric metamaterial realization [35]. Due to the close proximity of adjacent piezoelectric patches, significant care was required during manufacturing to avoid any electrical connection between unit cells.

The waveguide was clamped at one end, and the pair of piezoelectric patches closest to the clamped end was used to excite the structure. A Polytec PSV-500 scanning laser Doppler vibrometer (SLDV) was used to obtain steady-state measurements of the out-of-plane velocity across the entire length of the metamaterial. A noise-burst voltage signal was generated by the SLDV and amplified using a Trek PZD350 amplifier before being applied to the input pair of piezos. A synthetic impedance system with 32 separately addressable shunt circuits was created using a National Instruments PXI chassis with four PXIe-7846R modules, resulting in a digital sample rate of 400 kHz. The analog part of the synthetic impedance circuit was realized on a printed circuit board that interfaces the controller to the piezoelectric shunt circuits. The printed circuit was designed to avoid crosstalk between unit cells, using a ground copper plane to avoid ground loops. To apply the numerically obtained inductance profile to the real waveguide, the numerical inductance values were re-scaled according to the measured capacitance of each unit cell to maintain the same electrical resonant frequency. The synthetic impedance system is programmed from a LabVIEW computer interface that allows the numerically obtained inductance values to be imported directly to the experimental system. The experimental setup is shown in Fig. 4. The velocity of the metamaterial and the voltage of each unit cell are shown in Fig. 5.

The experimental results of Fig. 5(a) are very similar to the numerical results in Fig. 3(a). Note that the frequency of maximum compression in the experimental results was 1263 Hz, which is 13 Hz higher than the expected value of 1250 Hz. Correspondingly, in Fig. 5(b), we show selected frequencies that are 13 Hz higher than those of Fig. 3(b). Notably, because the simulated system had no damping, the
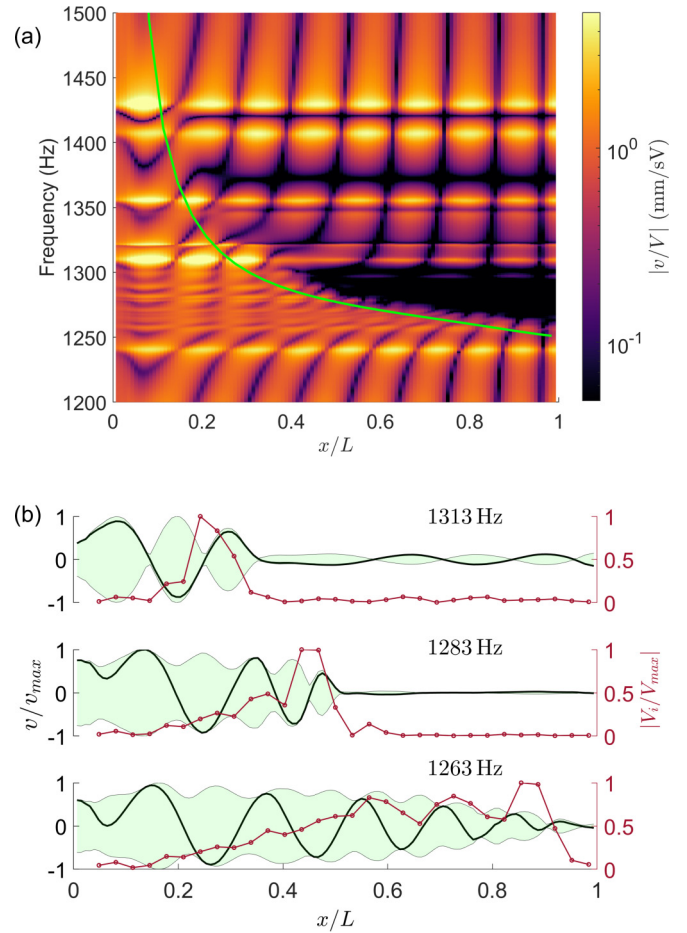

FIG. 5. (a) Measured steady-state response of the metamaterial vs position and frequency. The green line indicates the numerical resonant frequency profile which was applied to the experimental system. (b) Several highlighted velocity and voltage profiles at select frequencies of interest. The green shaded region shows the amplitude envelope of the metamaterial velocity, the black line shows an instantaneous velocity profile, and the red lines indicate the unit cell voltages at the specified frequency. Data is normalized to the maximum amplitude at that frequency.

experimental results show reduced wave compression compared to the numerical results. Nevertheless, just as in the simulated results, the voltage output of the unit cells gradually increases until the point of maximum compression, providing significant signal enhancement. Finally, this behavior is completely programmable, such that this signal amplification can be shifted in space, reversed, or recalculated to occur at a different operating frequency range.

IV. CONCLUSION

In this paper, we introduce a metamaterial waveguide with digital dispersion tailoring, enabling wave compression and signal enhancement at user-defined position and frequency. The system is analogous to a reconfigurable acoustic black hole, using digital piezoelectric shunts to compress waves and increase voltage output in a specified location. As a sensor array, the piezoelectric metamaterial is capable of isolating

specific frequencies and positions of interest, increasing sensitivity by gradually varying dispersion properties and avoiding sudden changes and unwanted reflections. More broadly, the system is capable of nearly arbitrary spatial variation of the wave speed (and hence the refractive index), marking a significant step toward fully programmable wave devices. Extensions to 2D or 3D can enable the creation of digitally programmable and reconfigurable gradient-index lenses [36] for enhanced sensing, energy harvesting, and power delivery.

[1] Z. Liu, X. Zhang, Y. Mao, Y. Y. Zhu, Z. Yang, C. T. Chan, and P. Sheng, Locally resonant sonic materials, Science **289**, 1734 (2000).

[2] H. Huang, C. Sun, and G. Huang, On the negative effective mass density in acoustic metamaterials, Int. J. Eng. Sci. **47**, 610 (2009).

[3] C. Sugino, Y. Xia, S. Leadenham, M. Ruzzene, and A. Erturk, A general theory for bandgap estimation in locally resonant metastructures, J. Sound Vib. **406**, 104 (2017).

[4] N. Fang, D. Xi, J. Xu, M. Ambati, W. Srituravanich, C. Sun, and X. Zhang, Ultrasonic metamaterials with negative modulus, Nat. Mater. **5**, 452 (2006).

[5] S. H. Lee, C. M. Park, Y. M. Seo, Z. G. Wang, and C. K. Kim, Acoustic metamaterial with negative modulus, J. Phys.: Condens. Matter **21**, 175704 (2009).

[6] C. Sugino, S. Leadenham, M. Ruzzene, and A. Erturk, An investigation of electroelastic bandgap formation in locally resonant piezoelectric metastructures, Smart Mater. Struct. **26**, 055029 (2017).

[7] Y. Ding, Z. Liu, C. Qiu, and J. Shi, Metamaterial with Simultaneously Negative Bulk Modulus and Mass Density, Phys. Rev. Lett. **99**, 093904 (2007).

[8] N. I. Landy, S. Sajuyigbe, J. J. Mock, D. R. Smith, and W. J. Padilla, Perfect Metamaterial Absorber, Phys. Rev. Lett. **100**, 207402 (2008).

[9] D. R. Smith, J. J. Mock, A. F. Starr, and D. Schurig, Gradient index metamaterials, Phys. Rev. E **71**, 036609 (2005).

[10] N. Kundtz and D. R. Smith, Extreme-angle broadband metamaterial lens, Nat. Mater. **9**, 129 (2010).

[11] D. Cardella, P. Celli, and S. Gonella, Manipulating waves by distilling frequencies: A tunable shunt-enabled rainbow trap, Smart Mater. Struct. **25**, 085017 (2016).

[12] P. Celli, B. Yousefzadeh, C. Daraio, and S. Gonella, Bandgap widening by disorder in rainbow metamaterials, Appl. Phys. Lett. **114**, 091903 (2019).

[13] S. A. Cummer and D. Schurig, One path to acoustic cloaking, New J. Phys. **9**, 45 (2007).

[14] H. Chen and C. Chan, Acoustic cloaking in three dimensions using acoustic metamaterials, Appl. Phys. Lett. **91**, 183518 (2007).

[15] A. N. Norris, Acoustic cloaking theory, Proc. Roy. Soc. A: Math., Phys. Eng. Sci. **464**, 2411 (2008).

[16] M. Farhat, S. Guenneau, and S. Enoch, Ultrabroadband Elastic Cloaking in thin Plates, Phys. Rev. Lett. **103**, 024301 (2009).

[17] Y. Chen, H. Liu, M. Reilly, H. Bae, and M. Yu, Enhanced acoustic sensing through wave compression and pressure amplification in anisotropic metamaterials, Nat. Commun. **5**, 5247 (2014).

[18] V. Krylov and F. Tilman, Acoustic "black holes" for flexural waves as effective vibration dampers, J. Sound Vib. **274**, 605 (2004).

[19] V. V. Krylov and R. Winward, Experimental investigation of the acoustic black hole effect for flexural waves in tapered plates, J. Sound Vib. **300**, 43 (2007).

[20] A. Climente, D. Torrent, and J. Sánchez-Dehesa, Omnidirectional broadband acoustic absorber based on metamaterials, Appl. Phys. Lett. **100**, 144103 (2012).

[21] L. Zhao, S. C. Conlon, and F. Semperlotti, Broadband energy harvesting using acoustic black hole structural tailoring, Smart Mater. Struct. **23**, 065021 (2014).

[22] S. C. Conlon, J. B. Fahnline, and F. Semperlotti, Numerical analysis of the vibroacoustic properties of plates with embedded grids of acoustic black holes, J. Acoust. Soc. Am. **137**, 447 (2015).

[23] A. Pelat, F. Gautier, S. C. Conlon, and F. Semperlotti, The acoustic black hole: A review of theory and applications, J. Sound Vib. **476**, 115316 (2020).

[24] Y. Mi, W. Zhai, L. Cheng, C. Xi, and X. Yu, Wave trapping by acoustic black hole: Simultaneous reduction of sound reflection and transmission, Appl. Phys. Lett. **118**, 114101 (2021).

[25] O. Thorp, M. Ruzzene, and A. Baz, Attenuation and localization of wave propagation in rods with periodic shunted piezoelectric patches, Smart Mater. Struct. **10**, 979 (2001).

[26] F. Casadei, M. Ruzzene, L. Dozio, and K. A. Cunefare, Broadband vibration control through periodic arrays of resonant shunts: Experimental investigation on plates, Smart Mater. Struct. **19**, 015002 (2010).

[27] Y. Y. Chen, G. L. Huang, and C. T. Sun, Band gap control in an active elastic metamaterial with negative capacitance piezoelectric shunting, ASME. J. Vib. Acoust. **136**, 061008 (2014).

[28] C. Sugino, M. Ruzzene, and A. Erturk, An analytical framework for locally resonant piezoelectric metamaterial plates, Int. J. Solids Struct. **182-183**, 281 (2020).

[29] K. Yi, M. Collet, M. Ichchou, and L. Li, Flexural waves focusing through shunted piezoelectric patches, Smart Mater. Struct. **25**, 075007 (2016).

[30] Y. Chen, R. Zhu, M. Barnhart, and G. Huang, Enhanced flexural wave sensing by adaptive gradient-index metamaterials, Sci. Rep. **6**, 35048 (2016).

[31] A. J. Fleming, S. Behrens, and S. O. R. Moheimani, Synthetic impedance for implementation of piezoelectric shunt-damping circuits, Electron. Lett. **36**, 1525 (2000).

[32] G. Matten, M. Collet, S. Cogan, and E. Sadoulet-Reboul, Synthetic impedance for adaptive piezoelectric metacomposite, Procedia Technol. **15**, 84 (2014).

[33] C. Sugino, M. Ruzzene, and A. Erturk, Digitally Programmable Resonant Elastic Metamaterials, Phys. Rev. Appl. **13**, 061001(R) (2020).

[34] K. Yi, G. Matten, M. Ouisse, E. Sadoulet-Reboul, M. Collet, and G. Chevallier, Programmable metamaterials with digital synthetic impedance circuits for vibration control, Smart Mater. Struct. **29**, 035005 (2020).

[35] M. Alshaqaq, C. Sugino, and A. Erturk, Programmable Rainbow Trapping and Band-Gap Enhancement via Spatial Group-Velocity Tailoring in Elastic Metamaterials, Phys. Rev. Appl. **17**, L021003 (2022).

[36] S. Tol, F. L. Degertekin, and A. Erturk, Gradient-index phononic crystal lens-based enhancement of elastic wave energy harvesting, Appl. Phys. Lett. **109**, 063902 (2016).